Ab initio study of the ferroelectric strain dependence and 180° domain walls in the barium metal fluorides $BaMgF_4$ and $BaZnF_4$

Maribel Núñez Valdez*
Materials Theory, ETH Zürich, Wolfgang-Pauli-Strasse 27, CH-8093 Zürich, Switzerland and Moscow Institute of Physics and Technology, Dolgoprudny, Moscow Region, Russia

Hendrik Th. Spanke and Nicola A. Spaldin
Materials Theory, ETH Zürich, Wolfgang-Pauli-Strasse 27, CH-8093 Zürich, Switzerland
(Received 10 November 2015; published 17 February 2016)

We investigate the strain dependence of the ferroelectric polarization and the structure of the ferroelectric domain walls in the layered perovskite-related barium fluorides, $BaMF_4$ (M = Mg, Zn). The unusual "geometric ferroelectricity" in these materials is driven by the softening of a single polar phonon mode consisting of rotations of the MF_6 octahedra accompanied by polar displacements of the Ba cations, and in contrast to conventional ferroelectrics involves minimal electronic rehybridization. We therefore anticipate a different strain dependence of the polarization, and alternative domain wall structures compared with those found in conventional ferroelectric materials. Using first-principles calculations based on density functional theory (DFT) within the general gradient approximation (GGA), we calculate the variation of the crystal structure and the ferroelectric polarization under both compressive and tensile strain. We perform structural relaxations of neutral domain walls between oppositely oriented directions of the ferroelectric polarization and calculate their corresponding energies to determine which are most likely to form. We compare our results to literature values for conventional perovskite oxides to provide a source of comparison for understanding the ferroelectric properties of alternative nonoxide materials such as the barium fluorides.

DOI: 10.1103/PhysRevB.93.064112

I. INTRODUCTION

Ferroelectric and multiferroic oxides are widely studied because of their fundamental interest and for technological applications such as nonvolatile random access memories [1], piezoelectric actuators and sensors [2], pyroelectric detectors [3], and electro-optic and nonlinear optical devices [4]. Indeed, it is often assumed that the presence of oxygen, which forms highly polarizable bonds with transition metal cations, is a requirement for good ferroelectric behavior. Recently, however, research on ferroelectric materials based on alternative chemistries without oxygen has received renewed interest. In particular, the class of barium metal fluorides, $BaMF_4$ (for a review see Ref. [5] and references therein), such as $BaMgF_4$ [6] could prove to be important because of the wide band gaps and associated transparency of fluorine-based compounds, which makes them attractive for advanced photonic and optoelectronic applications [7].

The $BaMF_4$ barium metal fluorides form in a bilayered, perovskite-related base-centered orthorhombic structure (space group No. 36, $Cmc2_1$) as shown in Fig. 1. The divalent M cation can be a 3d transition metal ion (Mn, Fe, Co, or Ni) or a nonmagnetic divalent ion (Mg or Zn), and is octahedrally coordinated by fluorine anions. Two-layer slabs of corner-sharing MF_6 octahedra lie perpendicular to the crystallographic b axis with Ba cations in planes between the slabs [9,10]. The structure is polar, and ferroelectric switching using a pulsed-field technique has been demonstrated at room temperature for all members of the $BaMF_4$ family except for M = Mn and Fe [5,10]. The high-temperature paraelectric reference phase has not been identified experimentally, because melting occurs before the ferroelectric Curie temperature T_C (estimated to be between 1100 and 1600 K by extrapolating the temperature-dependent dielectric constants [11]) is reached. First-principles electronic structure calculations have shown, however, that the ferroelectric ground state can be reached from a prototypical centrosymmetric $Cmcm$ structure [Fig. 1(d)] via a single polar phonon mode which consists of a rotation of the MF_6 octahedra accompanied by a displacement of the Ba^{2+} atoms along the b axis [12]. The driving force for this so-called *geometric ferroelectricity* is the combination of size effects and the layered geometric coordination of the crystal lattice, rather than the usual electronic rehybridization found in conventional ferroelectrics. As a result, the Born effective charges, which reflect the degree of rehybridization during a polar distortion, are close to the formal ionic charges in contrast to the anomalously large values characteristic of conventional ferroelectrics. The same mechanism is believed to occur in the layered, perovskite-related rare-earth titanates $R_2Ti_2O_7$ [13,14]. A related improper version occurs in the hexagonal rare-earth manganites [15,16], and in so-called hybrid improper ferroelectrics [17,18], both of which also form layered structures.

We anticipate that this unconventional mechanism for the ferroelectric polarization in the $BaMF_4$ family might lead to quite different behavior in two properties that are particularly relevant for the incorporation of ferroelectrics into thin film devices. The first is the strain dependence of the ferroelectric polarization, which is particularly important when ferroelectrics are grown on substrates with mismatched lattice constants. The polarization-lattice coupling is substantial in many conventional oxide ferroelectrics [19], and is believed to be driven by the large electronic rehybridizations reflected

*Corresponding author: nunez_valdez.m@mipt.ru

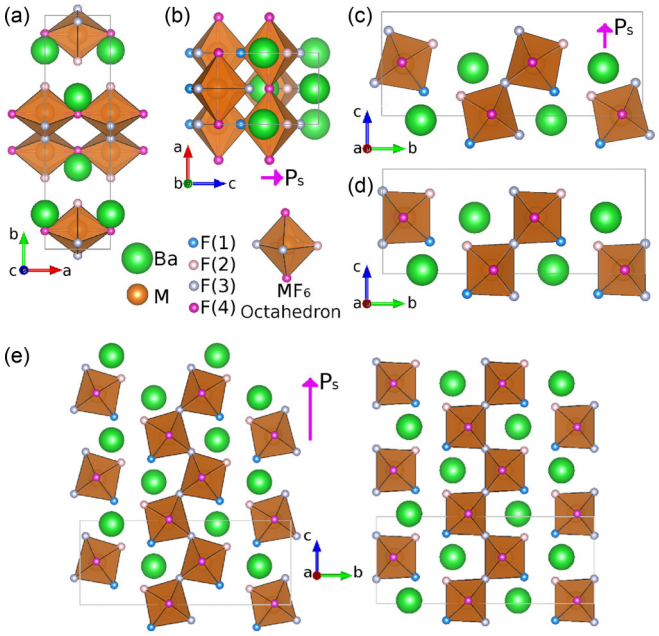

FIG. 1. Structure of $BaMgF_4$. (a)–(c) Ferroelectric $Cmc2_1$ phase in different orientations. The calculated lowest energy structure, which is similar to the experimental one, is shown. (d) Hypothetical $Cmcm$ centrosymmetric reference phase. (e) Comparison of the ground-state polar structure to the assumed centrosymmetric structure showing multiple unit cells with the direction of the spontaneous polarization P_S indicated. The ferroelectric and centrosymmetric structures of $BaZnF_4$ are qualitatively similar to those of $BaMgF_4$. The conventional primitive unit cell, which contains 24 atoms (four formula units), is indicated in gray. (All crystal visualizations in this paper were performed using VESTA [8].)

in the anomalous Born effective charges, therefore we expect smaller effects here. The second is the nature of the domain walls separating regions of opposite polarization. These have been studied extensively both theoretically and experimentally in conventional ferroelectric perovskite oxides because they have a profound influence on the material physical properties, in particular the ferroelectric hysteresis. The identity and structure of the lowest-energy domain walls in conventional perovskite oxides are now well established (see, for example, Refs. [20–23]). In addition, the interaction of domain walls with point defects such as oxygen vacancies, and the resulting effects on the properties are topics of tremendous current interest [24]. With the unusual rotational mechanism for ferroelectricity in $BaMF_4$, the domain walls might more closely resemble antiphase boundaries, with different energetics and thicknesses from their conventional ferroelectric counterparts. To the best of our knowledge, however, calculations exploring the strain dependence of polarization and the structure and properties of the domain walls in $BaMF_4$ ferroelectrics have not been performed; this is the goal of this work.

The remainder of this paper is organized as follows. In Sec. II, we describe the technical details of our calculations. Section III, the main part of the paper, contains our results for our two representative materials, $BaMgF_4$ and $BaZnF_4$. Specifically, we present the structures of the low-energy neutral domain walls obtained using structural optimizations of atomic positions, and the dependence of the spontaneous polarization on the strain. In Sec. IV, we summarize our main findings and present our conclusions.

II. COMPUTATIONAL DETAILS

Our calculations were performed using the Vienna *ab initio* simulation package (VASP) [25] within the projector-augmented plane wave (PAW) [26,27] method of density functional theory (DFT) [28,29]. We used the general-gradient approximation (GGA) in the prescription by Perdew, Burke, and Ernzerhof (PBE) [30] for the exchange-correlation potential. We used the default PAW potentials with the valence electronic configurations $5s^2\,5p^6\,6s^2$ for Ba, $3d^{10}\,4s^2$ for Zn, $3s^2$ for Mg, and $2s^2\,2p^5$ for F. A plane-wave cutoff energy of 500 eV and a Brillouin-zone k-point sampling of $6\times4\times6$ within the 24-atom unit cell were used. Convergence was assumed when the forces on each atom were smaller than 1 meV/Å and the total energy changes less than 10^{-8} eV. The electronic contributions to the spontaneous polarization (P_S), defined as the difference in polarization between the ferroelectric ground state structure ($Cmc2_1$) and the postulated high symmetry paraelectric phase ($Cmcm$), were calculated using the Berry phase approach [31–33] by integrating over six homogeneously distributed k-point strings, parallel to the reciprocal crystallographic c axis, each containing ten k points.

III. RESULTS

A. Structural, electronic, and ferroelectric properties

We begin by calculating the lowest energy structures and lattice parameters for the bulk ferroelectric ($Cmc2_1$) phases of $BaMgF_4$ and $BaZnF_4$. Our 0 K results, shown in Table I, compare reasonably with experimental measurements at ∼10 K extracted from synchrotron powder diffraction data [34] and a previous DFT calculation for $BaZnF_4$ [35]. Our calculated atomic positions are in good agreement with the experimentally determined positions along the a and b directions, with larger deviations in the c direction. Likewise our a and c lattice parameters are close to the measured values, with a difference of ∼2.5% for the b lattice parameter perpendicular to the layers, likely due to the GGA overestimating the weak bonding between the layers.

In Fig. 2, we show our calculated densities of states. We see that both compounds are strongly insulating with large DFT band gaps (6.9 and 4.5 eV for $BaMgF_4$ and $BaZnF_4$ respectively). The top of the valence bands is formed primarily from F $2p$ states and the lower part of the conduction bands from Ba $5d$ states, with negligible hybridization between them. A notable difference between the two materials is the presence of Zn $3d$ states mixed with the F $2p$ states at the bottom of the valence band in $BaZnF_4$, and Zn $4s$ states at the bottom of the conduction band leading to the smaller gap in this case. Mg s states are minimally present in the range shown.

Figure 3 shows the dependence of the total energy per formula unit (f.u.) on the pattern of atomic displacements that transforms the paraelectric (PE) structure to the ground state ferroelectric (FE) structure for $BaMgF_4$. We see the usual double-well potential characteristic of proper ferroelectrics with an energy barrier, ΔE, between the two equivalent

TABLE I. Our calculated structural parameters [*] at zero temperature for the $Cmc2_1$ ferroelectric phases of $BaMgF_4$ and $BaZnF_4$. Experimental data at 10 K from Ref. [34] for both materials, and DFT results from Ref. [35] for $BaZnF_4$ are shown for comparison. All atomic positions have Wyckoff symmetry 4*a*.

		Mg		Zn		
		DFT	EXP	DFT		EXP
Parameter		[*]	Ref. [34]	[*]	Ref. [35]	Ref. [34]
a_0 (Å)		4.16	4.119	4.25	4.281	4.191
b_0 (Å)		14.83	14.463	14.88	14.700	14.513
c_0 (Å)		5.93	5.812	5.97	5.921	5.835
Ba	*x*	0.5	0.5	0.5	0.5	0.5
	y	0.350	0.351	0.351	0.3520	0.352
	z	0.460	0.536	0.455	0.4575	0.537
M	*x*	0.0	0.0	0.0	0.0	0.0
	y	0.416	0.414	0.414	0.413	0.413
	z	0.002	0.0	−0.002	0.0	0.0
F(1)	*x*	0.0	0.0	0.0	0.0	0.0
	y	0.338	0.306	0.335	0.333	0.303
	z	0.734	0.803	0.726	0.727	0.800
F(2)	*x*	0.0	0.0	0.0	0.0	0.0
	y	0.304	0.334	0.302	0.301	0.330
	z	0.191	0.261	0.193	0.198	0.262
F(3)	*x*	0.0	0.0	0.0	0.0	0.0
	y	0.527	0.473	0.531	0.531	0.471
	z	0.817	0.692	0.831	0.830	0.673
F(4)	*x*	0.5	0.5	0.5	0.5	0.5
	y	0.422	0.422	0.423	0.423	0.422
	z	0.015	−0.010	0.017	0.017	0.983

ferroic ground states of 0.133 eV/f.u.; the corresponding barrier for $BaZnF_4$ is 0.218 eV/f.u. For comparison, in the magnetic members of this fluoride family, with M = Mn, Fe, Co, and Ni, ΔE ranges from ∼0.025 to ∼0.2 eV/f.u.

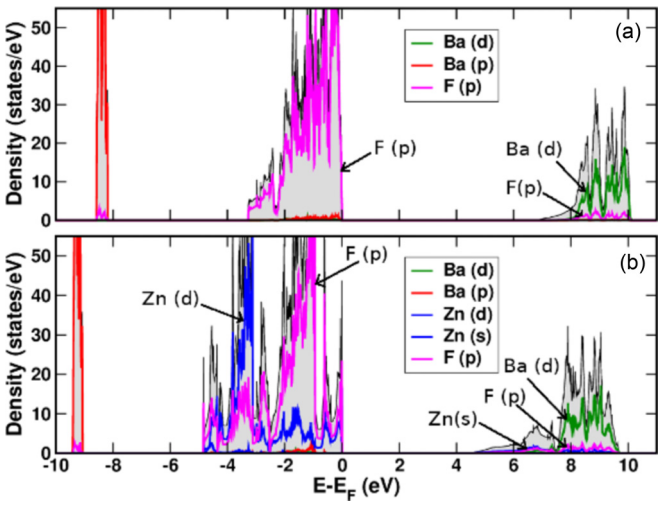

FIG. 2. Total (black line and gray shaded) and partial (color) densities of states of bulk (a) $BaMgF_4$ and (b) $BaZnF_4$. Ba *p* states are shown in red, Ba *d* states in green, and F *p* states in magenta. Zn *d* and *s* states are in blue.

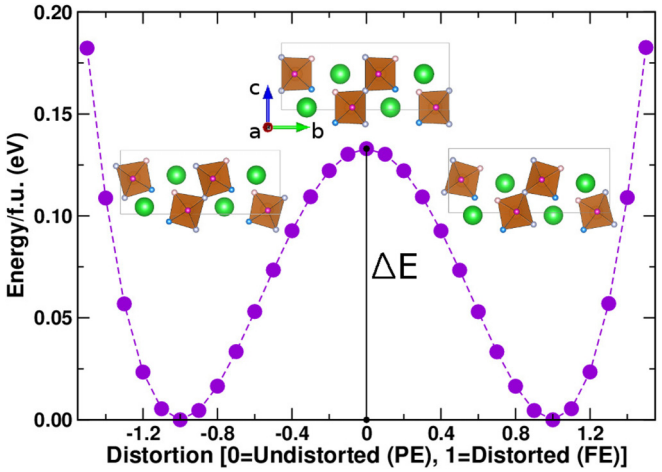

FIG. 3. Energy per formula unit (f.u.) of $BaMgF_4$ as a function of the magnitude of the ferroelectric structural distortion. For $BaZnF_4$ the form of the double-well potential is qualitatively similar but the energy barrier, ΔE, is larger. The left and right insets show the MgF_6 octahedral rotation patterns in the two ferroic ground states compared to the unrotated PE phase (central inset).

[12]; the conventional oxide perovskite ferroelectrics $BaTiO_3$ and $PbTiO_3$ have energy barriers of 0.018 and 0.200 eV/f.u. respectively [36].

Our calculated spontaneous polarizations P_S, obtained from the difference in polarization between the undistorted $Cmcm$ PE phase and the $Cmc2_1$ FE ground state along the same branch of the polarization lattice, are shown in Table II. First, we note that our calculations give polarization values that are consistently somewhat larger than the experimentally reported values. To check whether this is a consequence of our choice of exchange correlation functional, we repeated our calculations using the PBEsol functional and found a similar overestimate. We suggest, therefore, that the lower experimental values might be the result of incomplete switching. [Note that use of the local density approximation (LDA) to describe the exchange and correlation gives poor agreement between experimental and calculated lattice parameters and so we do not include it here.] Next, we see that the values obtained using the Berry phase approach are similar to those obtained from multiplying the displacements of the ions with their formal ionic point charges (Ba^{2+}, M^{2+}, F^-), indicating that the Born

TABLE II. Spontaneous polarizations calculated by summing over the product of the formal charges times the displacements, using the Berry phase approach, and measured experimentally (‡Ref. [11], †Ref. [37], and ⋆Ref. [38]).

P_S (001)		$BaMgF_4$ $\mu C/cm^2$	$BaZnF_4$ $\mu C/cm^2$
Formal charges	PBE	8.9	11.4
	PBEsol	9.2	11.2
Berry phase	PBE	10.1	13.2
	PBEsol	10.5	13.0
Experimental		7.7‡	9.7‡
		6.9†	9.0⋆

effective charges, Z^*, are close to their formal values and that the ferroelectric mechanism is of geometric nature with no significant charge transfer between cations and anions [12]. In closing this section and as stated above, we expect that these nonanomalous Born effective charges might lead to a different strain-polarization coupling from that found in conventional ferroelectrics and we investigate this next.

B. Effect of strain on the ferroelectric polarization

The thin film geometry, in which a ∼1-nm-thick layer of ferroelectric material is grown on a substrate or metallic electrode, is important in device architectures, and can be used to modify the ferroelectric behavior through strain induced via coherent heteroepitaxy with the substrate. In conventional perovskite ferroelectrics such strain-polarization coupling can be strong, leading, for example, to the onset of ferroelectricity in otherwise paraelectric $SrTiO_3$ [39] and the enhancement of the polarization and coercivity in ferroelectric $BaTiO_3$ [40]. First-principles studies [19] have rationalized the magnitude of the strain dependence in terms of the material's piezoelectric and elastic constants, which in turn are often large in oxide ferroelectrics. Motivated by these features, and by the different nature of the ferroelectric polarization in the fluoride compounds, we now calculate the strain dependence of the ferroelectric polarization for $BaMgF_4$ and $BaZnF_4$.

For our strain calculations, we use a 12-atom primitive cell, which is connected to the conventional unit cell through the relationships $\vec{a}' = \frac{1}{2}(a, -b, 2c)$, $\vec{b}' = \frac{1}{2}(a, b, 2c)$ and $\vec{c}' = \vec{c}$, see Fig. 4. This choice of system of reference is convenient because in this set up $|\vec{a}'| = |\vec{b}'|$. Strain is generated by fixing the lattice parameters corresponding to the lateral directions of the substrate (a' and b'), relaxing the internal ionic degrees of freedom, and determining the out-of-plane lattice parameter ($\vec{c}'$) by means of an equation of state. We induce compressive and tensile strains between -3% and $+3\%$, where the misfit strain is defined as $\varepsilon = \frac{|\vec{a}'|}{|\vec{a}'_0|} - 1 = \frac{|\vec{b}'|}{|\vec{b}'_0|} - 1$. Note that in this orientation the ferroelectric polarization lies perpendicular to the plane of the film, a geometry that is desirable for device applications but in practice might be difficult to achieve through conventional layer-by-layer growth methods.

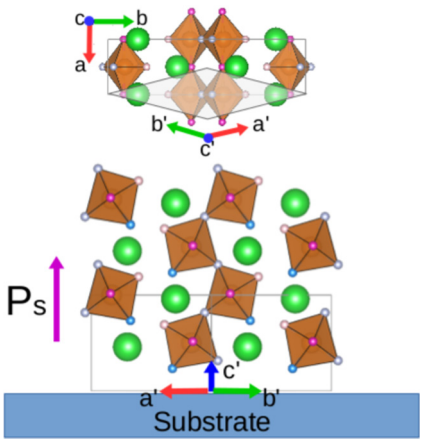

FIG. 4. Orientation of BaMF$_4$ relative to the substrate adopted in this work. The 12-atom primitive cell is indicated and compared to the 24 atom cell (top figure).

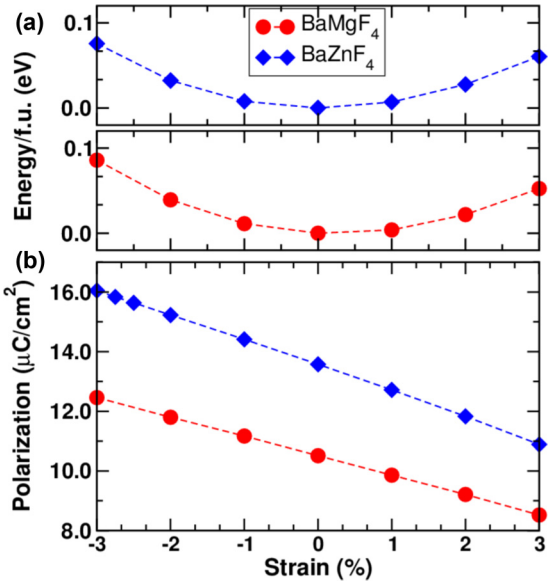

FIG. 5. (a) Energy per formula unit (f.u.) and (b) spontaneous polarization P_S as a function of strain ($\varepsilon = |\vec{a}'|/|\vec{a}'_0| - 1 = |\vec{b}'|/|\vec{b}'_0| - 1$) calculated using the Berry phase approach for BaMF$_4$ (M = Mg, Zn).

Our calculated internal energies and polarizations as a function of strain are shown in Fig. 5. The energy variations over the ± 3% strain range are less than 0.3% for compressive strain and 0.1% for tensile strain with respect to the zero-strain energy [Fig. 5(a)]. Then, we note that the polarization direction remains along the out-of-plane crystallographic c axis for all strain values studied, in contrast to many perovskite oxides in which the polarization becomes in plane for tensile strain. It also contrasts with the case of the hybrid improper ferroelectric $CaTiO_3$, for which compressive strain drives the polarization in plane [41]. Indeed, the spontaneous polarization varies close to linearly with strain for the entire range considered, with variations in magnitude from around +20% to −15% for both compounds compared to their unstrained values. While less dramatic than in some oxide counterparts, these values are not insignificant and should not be ignored in creating heterostructures with lattice-mismatched materials. It is also in contrast to the behavior found in calculations for hybrid improper ferroelectric superlattices, such as R_2NiMnO_6/La_2NiMnO_6 (where R is a rare-earth ion), in which the polarization is essentially independent of the epitaxial strain [42] or $LaScO_3/BiScO_3$, which show a discontinuous increase in polarization as a function of strain [43]. This nearly linear response of the spontaneous polarization to strain ϵ indicates that the barium fluorides also satisfy the relationship discussed for conventional ferroelectrics in Ref. [19] that

$$\Delta P = \left(2c_{31} - \frac{c_{33}}{n}\right)\epsilon = c_{\text{eff}}\epsilon. \quad (1)$$

Here, ΔP is the change in polarization, c_{31} and c_{33} are components of the piezoelectric tensor, and n is the Poisson ratio. Our effective piezoelectric constants, c_{eff}, are −65 and −86 μC/cm^2 for $BaMgF_4$ and $BaZnF_4$, respectively, comparable to that of rhombohedral $BiFeO_3(R3c)$ (−85 μC/cm^2) but an order of magnitude smaller than those of $BaTiO_3$ and

$PbTiO_3$. Our calculated electronic band structures (not shown) indicate minimal change in band gap with strain.

C. Ferroelectric domains: formation of 180° domain walls

The domain walls between regions of differently oriented polarization in ferroelectrics are known to influence the ferroelectric switching behavior as well as to have functional properties in their own right [44,45]. Much is known about the structure and energetics of domain walls in perovskite oxide ferroelectrics, both from first-principles density functional calculations (see, for example, Refs. [23,46–49]) and from detailed experimental studies using for example high-resolution transmission electron microscopy (see, for example, Refs. [50,51]). However, information about ferroelectric domain walls in the BaMF$_4$ compounds is to our knowledge completely lacking; we provide the first calculations here.

In most domain walls, the component of polarization perpendicular to the wall is constant, so that

$$(\mathbf{P}_A - \mathbf{P}_B) \cdot \mathbf{n} = 0, \tag{2}$$

where $\mathbf{P}_A$ and $\mathbf{P}_B$ are the spontaneous polarizations of the two domains. This condition avoids a divergence of the electrostatic potential, which would require a screening by additional charges and so such walls are called neutral (as opposed to charged) domain walls. In this work we restrict our discussion to neutral domain walls. In addition, we consider only 180° domain walls, in which the orientation of the polarization changes by 180° across the wall, and leave for other orientations such as 90° domain walls for future investigation. We explore two geometries, with the normal vector $\mathbf{n}$ parallel to the crystallographic a and b axes in turn. To calculate the domain wall structures and energetics, we construct supercells of the form $1\times4\times1$ times the primitive unit cell (containing 96 atoms) and $6\times1\times1$ times the primitive unit cell (144 atoms) for walls parallel to the ac and bc planes; we refer to these hereafter as (101)-DWs and (011)-DWs, respectively. Within each supercell we impose two oppositely oriented domains with polarization parallel and antiparallel to the c axis and two domain walls. The central slabs of each domain are constrained to their calculated bulk ferroelectric structures (see Fig. 6). We then relax the atoms in the wall regions to their lowest-energy configurations using the same convergence criteria as in Sec. II. The energy of a domain wall is then given by

$$E_{\text{domain wall}} = \frac{E - E_0}{2S}, \tag{3}$$

where E is the total energy of the supercell configuration in the presence of domain walls, E_0 is the reference energy of bulk BaMF$_4$ (computed for the same corresponding supercell), and S is the area of the domain wall (of which there are two per supercell). The convergence of the domain wall energies with respect to supercell size was tested by adopting different sizes with 72 and 96 atoms for the (101)-, and 96, 120, and 144 atoms for the (011)-DW configurations. The (011)-DWs converged more slowly and required larger supercells due to the corner sharing of the octahedra perpendicular to the domain wall. Table III shows our calculated energies for the two domain wall configurations investigated here as well as literature values for other selected ferroelectrics.

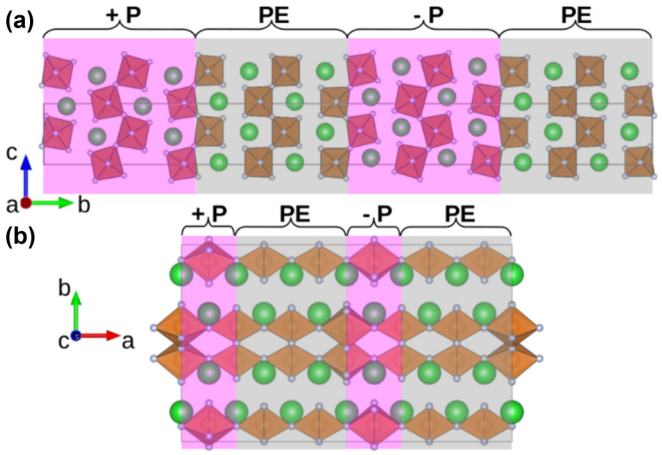

FIG. 6. Starting (a) (101)-DW and (b) (011)-DW configurations for $BaMgF_4$ (for $BaZnF_4$ the setup is analogous). We show two supercells along the c direction in (a) only to help with visualization. Ions in PE regions (including the ones directly at the boundaries) are allowed to relax from the initial PE positions. The other regions have polarizations fixed along $+P$ and $-P$, respectively.

We see that the domain wall energies of the fluorides are similar to those of the oxides but we find no clear correlation between Curie temperature, magnitude of ferroelectric polarization, and domain wall energies for either the conventional ferroelectric perovskites or the geometric ferroelectric compounds.

We find that the domain wall energy is lowest for the (101)-DW configuration in $BaMgF_4$ and for the (011)-DW configuration in $BaZnF_4$ (although in the latter case the energies of the two wall types are very close). We attribute this difference to the chemical activity of the Zn $3d$ electrons, although a detailed explanation is still lacking.

In Fig. 7, we show our calculated layer-by-layer polarizations perpendicular to the wall direction obtained from

$$P = \frac{e}{\Omega} \sum_{\alpha} Z_\alpha \cdot u_\alpha. \tag{4}$$

Here, e is the charge of the electron, Ω the volume of a $1\times1\times1$-cell layer, u_α is the displacement of atom α from its paraelectric position in the z direction, Z_α are the formal ionic

TABLE III. Domain wall energies calculated in this work for the (101)-DW (†) and (011)-DW (‡) configurations of $BaMgF_4$ and $BaZnF_4$, as well as the oxide ferroelectrics $BiFeO_3$, $PbTiO_3$ and hexagonal $YMnO_3$. The measured Curie temperatures and calculated polarizations are also shown for comparison. (References: ⋆-this work, ∗-[11], a-[52], b-[46,48], c-[53], d-[23], e-[54], f-[55], and g-[47].)

Material	T_C (K)	P_S (μC/cm^2)	$E_{\text{domain wall}}$ (mJ/m^2)
$BaMgF_4$	1263*	10.1	72†
			148‡
$BaZnF_4$	1083*	13.2	185†
			159‡
$BiFeO_3$	1103_a	90_a	80-800$_b$
$PbTiO_3$	765_c	75_c	132_d
h-$YMnO_3$	1258_e	5.6_f	11_g

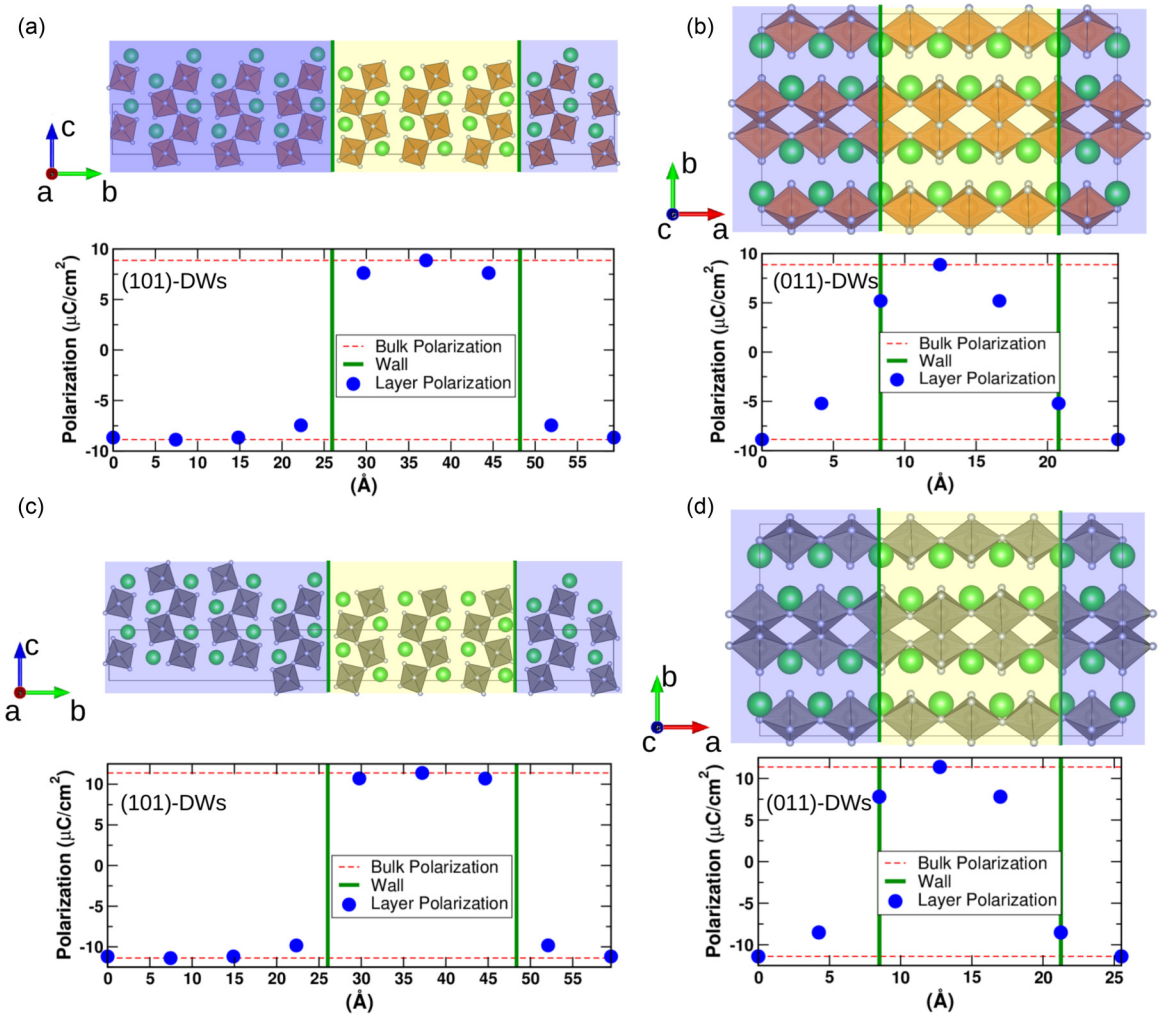

FIG. 7. Layer Polarization in the (101)-DW and (011)-DW configurations for (a) and (c) $BaMgF_4$ and (b) and (d) $BaZnF_4$, respectively.

charges and the index α runs over all atoms in the considered $1\times1\times1$-cell layer. Figures 7(a) and 7(b) show our results for $BaMgF_4$ and Figs. 7(c) and 7(d) for $BaZnF_4$. We find that the (101)-DW domain walls are sharp [Figs. 7(a) and 7(c)], that is, the local polarization changes abruptly across the domain wall from one bulk value to the opposite value. In contrast, our calculated lowest energy (011)-DW walls [Figs. 7(b) and 7(d)] show a smoother change in polarization across the wall. We can rationalize the difference in wall widths from the connectivity of the layers: while in the (101)-DW structures the wall lies between planes of MF_6 octahedra, in the (011)-DW the walls cut through the planes enforcing a gradual change of polarization across the wall. We note also that for both wall geometries, the MgF_6 octahedra retain their regular shape, but the ZnF_6 octahedra distort across the wall, particularly in the (011)-DW structure.

We point out that such atomically sharp domain walls are also observed in the improper ferroelectric hexagonal $YMnO_3$ series [47,51] where they have been compared to the narrow twin planes formed at anti-phase boundaries in antiferrodistortive materials. Here the physics is similar, although the $BaMF_4$ series represents an unusual example of the behavior in a *proper* ferroelectric. In conventional ferroelectric perovskite oxides, while ferroelectric domain walls tend to be narrow, they are not atomically sharp.

IV. SUMMARY

In summary, using first-principles density functional theory we have calculated two properties of $BaMgF_4$ and $BaZnF_4$ that are relevant for their behavior in ferroelectric thin films. First, we calculated the strain dependence of the spontaneous polarization and found that it varies close to linearly with both compressive and tensile strain indicating that it can be tuned in coherent thin-film heterostructures by appropriate choice of substrate lattice constant. Next, we calculated the energies and structures of neutral 180° domain walls and identified those most likely to occur in practical samples. We found that the domain wall energies are comparable to those of conventional oxide ferroelectrics, but that the wall thicknesses are thinner, reminiscent of twin boundaries in antiferrodistortive materials. We hope that our study motivates further experimental investigation of the $BaMF_4$ class of materials, and other unconventional ferroelectrics with octahedral rotations, such as hybrid improper ferroelectrics, for which, to our knowledge, only one study of a domain wall exists [43].

ACKNOWLEDGMENTS

This work was supported by ETH Zürich and by the ERC Advanced Grant program, No. 291151. Computations were performed at the Swiss Supercomputing Center and on the ETH Zürich Brutus cluster; final computational details and manuscript writing were completed at MIPT ("5top100" fellowship). The authors thank J. F. Scott and J. M. Rondinelli for useful discussions.

[1] O. Auciello, J. F. Scott, and R. Ramesh, Phys. Today **51**, 22 (1998).
[2] P. Muralt, J. Micromech. Microeng. **10**, 136 (2000).
[3] Q. Zhang and R. W. Whatmore, J. Appl. Phys. **94**, 5228 (2003).
[4] B. W. Bessels, Annu. Rev. Mater. Res. **37**, 659 (2007).
[5] J. F. Scott, Rep. Prog. Phys. **42**, 1055 (1979).
[6] S. C. Buchter, T. Y. Fan, V. Liberman, J. J. Zayhowski, M. Rothschild, E. J. Mason, A. Gassanho, H. P. Jenssen, and J. H. Burnett, Opt. Lett. **26**, 1693 (2001).
[7] J. P. Meyn and M. Fejer, Opt. Lett. **22**, 1214 (1997).
[8] K. Momma and F. Izumi, J. Appl. Cryst. **41**, 653 (2008).
[9] H. G. v. Schnering and P. Bleckmann, Naturwiss. **55**, 342 (1968).
[10] M. Eibschütz, H. J. Guggenheim, S. H. Wemple, I. Camlibel, and M. D. Jr., Phys. Lett. A **29**, 409 (1969).
[11] M. D. Jr., M. Eibschütz, H. J. Guggenheim, and I. Camlibel, Solid State Commun. **7**, 1119 (1969).
[12] C. Ederer and N. A. Spaldin, Phys. Rev. B **74**, 024102 (2006).
[13] J. López-Pérez and J. Íñiguez, Phys. Rev. B **84**, 075121 (2011).
[14] F. Lichtenberg, A. Herrnberger, and K. Wiedemann, Prog. Sol. Stat. Chem. **36**, 253 (2008).
[15] B. B. van Aken, T. T. M. Palstra, A. Filippetti, and N. A. Spaldin, Nat. Mater. **3**, 164 (2004).
[16] C. J. Fennie and K. M. Rabe, Phys. Rev. B **72**, 100103(R) (2005).
[17] N. A. Benedek and C. J. Fennie, Phys. Rev. Lett. **106**, 107204 (2011).
[18] J. M. Rondinelli and C. J. Fennie, Adv. Mater. **24**, 1961 (2012).
[19] C. Ederer and N. A. Spaldin, Phys. Rev. Lett. **95**, 257601 (2005).
[20] S. Stemmer, S. K. Streiffer, F. Ernst, and M. Rühle, Philos. Mag. A **71**, 713 (1995).
[21] S. K. Streiffer, C. B. Parker, A. E. Romanov, M. J. Lefevre, L. Zhao, J. S. Speck, W. Pompe, C. M. Foster, and G. R. Bai, J. Appl. Phys. **83**, 2742 (1998).
[22] J. Padilla, W. Zhong, and D. Vanderbilt, Phys. Rev. B **53**, R5969 (1996).
[23] B. Meyer and D. Vanderbilt, Phys. Rev. B **65**, 104111 (2002).
[24] C. Becher, L. Maurel, U. Aschauer, M. Lilienblum, C. Mag'en, D. Meier, E. Langenberg, M. Trassin, J. Blasco, I. P. Krug, P. A. Algarabel, N. A. Spaldin, J. A. Pardo, and M. Fiebig, Nat. Nanotechnol. **10**, 661 (2015).
[25] G. Kresse and J. Furthmüller, Phys. Rev. B **54**, 11169 (1996).
[26] P. E. Blöchl, Phys. Rev. B **50**, 17953 (1994).
[27] G. Kresse and D. Joubert, Phys. Rev. B **59**, 1758 (1999).
[28] P. Hohenberg and W. Kohn, Phys. Rev. **136**, B864 (1964).
[29] W. Kohn and L. J. Sham, Phys. Rev. **140**, A1133 (1964).
[30] J. P. Perdew, K. Burke, and M. Ernzerhof, Phys. Rev. Lett. **77**, 3865 (1996).
[31] R. D. King-Smith and D. Vanderbilt, Phys. Rev. B **47**, 1651 (1993).
[32] D. Vanderbilt and R. D. King-Smith, Phys. Rev. B **48**, 4442 (1993).
[33] R. Resta, Rev. Mod. Phys. **66**, 899 (1994).
[34] J. M. Posse, A. Grzechnik, and K. Friese, Acta Cryst. B **265**, 576 (2009).
[35] D. Cao, M. Q. Cai, C. H. Tang, P. Yu, W. Y. Hu, Y. Du, B. Y. Huang, and H. Q. Deng, Eur. Phys. J. B **74**, 447 (2010).
[36] R. E. Cohen, Nature (London) **358**, 136 (1992).
[37] C. V. Kannan, K. Shimamura, H. R. Zeng, H. Kimura, E. G. Villora, and K. Kitamura, J. Appl. Phys. **104**, 114113 (2008).
[38] E. G. Villora, K. Shimamura, F. Jing, and A. Medvedev, Appl. Phys. Lett. **90**, 192909 (2007).
[39] J. H. Haeni, P. Irvin, W. Chang, R. Uecker, P. Reiche, Y. L. Li, S. Choudhury, W. Tian, M. E. Hawley, B. Craigo, A. K. Tagantsev, X. Q. Pan, S. K. Streiffer, L. Q. Chen, S. W. Kirchoefer, J. Levy, and D. G. Schlom, Nature (London) **430**, 758 (2004).
[40] K. J. Choi, M. Biegalski, Y. L. Li, A. Sharan, J. Schubert, R. Uecker, P. Reiche, Y. B. Chen, X. Q. Pan, V. Gopalan, L.-Q. Chen, D. G. Schlom, and C. B. Eom, Science **306**, 1005 (2004).
[41] Q. Zhou and K. M. Rabe, arXiv:1306.1839v2.
[42] H. J. Zhao, W. Ren, Y. Yang, J. Íñiguez, X. M. Chen, and L. Bellaiche, Nat. Commun. **5**, 4021 (2014).
[43] G. Gou and J. M. Rondinelli, Adv. Mater. Interfaces **1**, 201400042 (2014).
[44] J. Seidel, L. W. Martin, Q. He, Q. Zhan, Y.-H. Chu, A. Rother, M. Hawkridge, P. Maksymovych, P. Yu, M. Gajek, N. Balke, S. V. Kalinin, S. Gemming, H. Lichte, F. Wang, G. Catalan, J. F. Scott, N. A. Spaldin, J. Orenstein, and R. Ramesh, Nat. Mater. **8**, 229 (2009).
[45] D. Meier, J. Seidel, A. Cano, K. Delaney, Y. Kumagai, M. Mostovoy, N. A. Spaldin, R. Ramesh, and M. Fiebig, Nat. Mater. **11**, 284 (2012).
[46] A. Lubk, S. Gemming, and N. A. Spaldin, Phys. Rev. B **80**, 104110 (2009).
[47] Y. Kumagai and N. A. Spaldin, Nat. Commun. **4**, 1540 (2013).
[48] O. Diéguez, P. Aguado-Puente, J. Junquera, and J. Íñiguez, Phys. Rev. B **87**, 024102 (2013).
[49] W. Ren, Y. Yang, O. Diéguez, J. Íñiguez, N. Choudhury, and L. Bellaiche, Phys, Rev. Lett. **110**, 187601 (2013).
[50] C. L. Jia, K. W. Urban, M. Alexe, D. Hesse, and I. Vrejoiu, Science **331**, 1420 (2011).
[51] Q. H. Zhang, L. J. Wang, X. K. Wei, R. C. Yu, L. Gu, A. Hirata, M. W. Chen, C. Q. Jin, Y. Yao, Y. G. Wang, and X. F. Duan, Phys. Rev. B **85**, 020102(R) (2012).
[52] J. Wang, J. B. Neaton, H. Zheng, V. Nagarajan, S. B. Ogale, B. Liu, D. Viehland, V. Vaithyanathan, D. G. Schlom, U. V. Waghmare, N. A. Spaldin, K. M. Rabe, M. Wuttig, and R. Ramesh, Science **299**, 1719 (2003).
[53] B. Jaffe, W. R. Cook, and H. Jaffe, *Non-Metallic Solids*, Vol. 3 (Academic Press, London, New York, 1971).
[54] A. S. Gibbs, K. S. Knight, and P. Lightfoot, Phys. Rev. B **83**, 094111 (2011).
[55] N. Fujimura, T. Ishida, T. Yoshimura, and T. Ito, Appl. Phys. Lett. **69**, 1011 (1996).